New insights of fCO_2 variability in the tropical eastern Pacific Ocean using SMOS SSS

C. Walker Brown[1], J. Boutin[1], L. Merlivat[1]

[1]{ Sorbonne Universités (UPMC, Univ Paris 06)-CNRS-IRD-MNHN, LOCEAN Laboratory, 4 place Jussieu, F-75005, Paris, France}

Correspondence to: Christopher Walker Brown (christopher.brown@locean-ipsl.upmc.fr)

Abstract

Complex oceanic circulation and air-sea interaction make the eastern tropical Pacific Ocean (ETPO) a highly variable source of CO_2 to the atmosphere. Although the scientific community have amassed 70,000 surface fugacities of carbon dioxide (fCO_2) datapoints within the ETPO region over the past 25 years, the spatial and temporal resolution of this dataset is insufficient to fully quantify the seasonal to inter-annual variability of the region, a region where fCO_2 has been observed to fluctuate by >300 μatm.

Upwelling and rainfall events dominate the surface physical and chemical characteristics of the ETPO, with both yielding unique signatures in sea surface temperature and salinity. Thus, we explore the potential of using a statistical description of fCO_2 within sea-surface salinity-temperature space. These SSS/SST relationships are based on in-situ SOCAT data collected within the ETPO. This statistical description is then applied to high resolution (0.25º) SMOS sea surface salinity and OSTIA sea surface temperature in order to compute regional fCO_2. As a result, we are able to resolve fCO_2 at sufficiently high resolution to elucidate the influence various physical processes have on the fCO_2 of the surface ETPO.

Normalised (to 2014) oceanic fCO_2 between July 2010 and June 2014 within the entire ETPO was 39 (+/-10.7) μatm supersaturated with respect to 2014 atmospheric partial pressures, and featured a CO_2 outgassing of 1.51 (+/- 0.41) mmol m^{-2} d^{-1}. Values of fCO_2 within the ETPO were found to be broadly split between southeast and a northwest regions. The north west, central and offshore regions were supersaturated, with wintertime wind jet driven upwelling found to be the first order control on fCO_2 values. This contrasts with the southeastern/ Gulf of Panama region, where heavy rainfall combined with rapid stratification of the upper water-column act to dilute dissolved inorganic carbon, and yield fCO_2 values undersaturated with respect to atmospheric fugacities of CO_2.

1. Introduction

Perturbations to the global carbon cycle caused by anthropogenically driven increases in atmospheric partial pressures of CO_2 (pCO_2) produce an acute requirement to understand inter-reservoir carbon fluxes (Le Quéré et al 2014). However, assessing these fluxes, especially the flux between the atmosphere and surface ocean is challenging, as pCO_2 within the oceanic reservoir varies considerably both spatially and temporally. Fortunately, considerable effort has been made in recording oceanic pCO_2 (or fugacity- fCO_2) over the past 50 years, with roughly 10 million individual measurements of global surface ocean pCO_2 taken, processed, flagged and assembled into two large datasets: the surface ocean CO_2 atlas (SOCAT) and Lamont-Doherty Earth Observatory (LDEO) carbon dioxide database (Bakker et al., 2014; Takahashi et al., 2014). Both databases make heavy use of 'vessel of opportunity' derived pCO_2 data, resulting in a heterogeneous dataset with the majority of measurements collected within the tight confines of commercial shipping lanes.

The first stage in efforts to estimate large scale air sea fluxes requires the extrapolation of these discrete surface pCO_2 observations over large areas of surface ocean. Completing a basic extrapolation of this vessel of opportunity based data results in a spatially-patchy pCO_2 field, as seen in the one degree gridded product available from SOCAT (Bakker et al., 2014). Therefore, in order to achieve improved spatial coverage, a frequently used solution is to fit data-driven diagnostic models (e.g. Feely et al. 2006; Park et al. 2010; Rödenbeck et al., 2013). These models use observed correlations between physical properties and the pCO_2 observed under these conditions. In addition, statistical criteria based on the surface ocean observations (for example, satellite imagery) and/ or neural networks have been used to identify biogeochemical provinces in order to improve the accuracy of the extrapolated field (Boutin et al. 1999; Cosca et al. 2003; Rangama et al., 2005; Landschützer et al., 2014). Although the quality of these extrapolation methods have been refined over the past few years, in part due to the increasing number of in situ measurements, the interannual variability of the global air-sea CO_2 flux obtained using different data-driven methods still substantially differ, and further work is required to unify our estimates and improve understanding of this air-sea flux.

The recent (2010-present) availability of sea surface salinity from the Soil Moisture Ocean

Salinity (SMOS) mission has provided a new tool in statistically modelled pCO_2 studies, as now the relationship between surface temperature, salinity, density and pCO_2 can be utilised in high resolution statistical descriptions of pCO_2 within TS space. It is this relationship that is explored within this paper in order to quantify inter and intra annual variability within the oceanographically complex eastern tropical Pacific Ocean (ETPO) region between 4 °N and 18 °N, and east of 95 °W (Fig. 1).

The ETPO region is influenced by northern and southern hemisphere trade winds, the doldrums, strong seasonal wind jets, heavy rainfall, strong solar heating and the El Nino- Southern Oscillation (ENSO), (Kessler, 2006). Within the ETPO the Intertropical Tropical Convergence Zone (ITCZ) is neither zonally oriented, nor spatially fixed over the course of a year, thus wind fields are highly variable in both strength and direction (Kessler, 2006). Further wind variability is introduced by low altitude jets blowing through three low elevation gaps in the Central American Cordillera, with these jets observed predominantly between November and February (Kessler 2002, Fig. 1-schematically represented by orange arrows). These strong jet winds are generated from the pressure gradient force resulting from high-pressure synoptic midlatitude weather systems transiting North America towards the low pressure Equatorial Pacific during the winter months (Chelton et al., 2001). Jet wind velocities of up to 20-30 ms^{-1} have been observed within the three gulfs, extending from the shoreline to at least 500 km into the ETPO (Chelton et al., 2001). The alignment of these jets is mainly meridional in the Gulf of Panama and Tehuantepec, and more zonal in the Gulf of Papagayo (Fig. 1). These jet winds result in strong wintertime upwelling in each of the three basins, with the northerly jet winds in the Gulfs of Tehuantepec and Panama promoting Ekman upwelling (Kessler, 2006). At 9 ˚N, 90 ˚W, the quasi permanent anticyclonic Costa Rica thermocline dome is energised by the westerly jet winds in the Gulf of Papagayo, again, resulting in upwelling (Fig 1. Kessler, 2002). However, the pressure disequilibrium that spawns these jet winds builds and subsides quickly (on a sub-weekly timescale), resulting in a highly fluctuating jet wind field, and nonlinearities in the oceanic (and hence upwelling) response to these episodic events (Kessler, 2006). Recent studies have shown that satellite SSS are very well suited to capture the variability of these high SSS events (Grodsky et al., 2014; Reul et al., 2013).

During summertime, these jet winds are rare, and the northward deflection of the ITCZ over the ETPO result in very high levels of precipitation, particularly within the Gulf of Panama (Fig. 1; Alory et al., 2012). The effect of this rainfall is a strong freshening and stratification of the surface, especially in the Gulf of Panama region. For this reason, the Gulf of Panama is often referred to as the 'Pacific freshpool', with salinities of <30 frequently observed (Alory et al., 2012).

2. Data and Methods

2.1 Observations of in-situ fCO_2 , DIC and atmospheric CO_2

We use SOCAT data as the basis of a statistical description of pCO_2 within the ETPO. All CO_2 data within the SOCAT database are recorded as fugacity of CO_2 (fCO_2); a measure of pCO_2 that is corrected for the non-ideal-gas behaviour carbon dioxide displays (Bakker et al., 2014). In this study we will use fugacity of CO_2, owing to the improved accuracy of this measure over pCO_2. The logistical importance of the region has proven beneficial, producing a large database of fCO_2/ SSS/SST observations, with ~ 70,000 surface carbon, temperature and salinity data-points collected between 1991 and 2011 (within the region depicted in Fig. 1). We use data (converted from pCO_2 to fCO_2) collected between 1991 and 2013 within the LDEO v2013 database as a semi-independent dataset to test our SOCAT based statistical description of fCO_2 within TS space (Takahashi et al. 2014). The LDEO database extends two years longer than SOCAT, making it a useful evaluation product.

In addition to surface fCO_2, we use dissolved inorganic carbon (DIC) concentrations within the ETPO measured during World Ocean Circulation Experiment cruise P19 in 1993 (Fig. 1, WOCE data available from http://cchdo.ucsd.edu/), and weekly dry-air CO_2 mole fractions (xCO_2) measured at Fanning Island (3.5° N, 159° W, as part of the Scripps CO2 program, http://scrippsco2.ucsd.edu/). We derive fCO_2 in the atmosphere according to:

$$fCO_{2\,air} = xCO_2\,(p_{atm}-p_{H2O}) \qquad (1)$$

Where P_{atm} is the atmospheric pressure taken from the ERA interim product (www.apps.ecmwf.int/datasets/) and $p_{H2O,}$ the saturated water pressure (Weiss, 1974).

2.2. Calculating air sea fluxes of CO_2

The air-sea flux of CO_2 (mmol m^{-2} d^{-1}) is derived using the difference between surface ocean and atmospheric fCO_2 values, the solubility of CO_2 in standard seawater ($\alpha\, CO_2$ calculated using the values given by Weiss 1974) and the gas transfer velocity kCO_2 (cm/h):

$$F= kCO_2\ \alpha CO_2\,(fCO_{2\,sea} - fCO_{2\,air}) \qquad (2)$$

k is calculated using the 10 metre wind speed based parameterisation described by Sweeney et al. 2007, where:

$$k=0.27U^2(660/Sc)^{0.5} \quad (3)$$

where Sc is the Schmidt number for CO_2 (Wanninkhof, 1992). We use the 0.25˚, daily resolution 10 m wind speed product from the Advanced Scatterometer (ASCAT, www.knmi.nl/scatterometer/), and air fCO_2 is calculated assuming water vapour saturation at the boundary layer, then using the description in Eq. 1.

We note that when calculating air-sea gas exchange, it is not practical to derive a unique k parameter for all oceanic conditions and locations of interest, therefore, through necessity, k is calculated using the non-specific parametrisation of Sweeney et al. 2007. Influences on k, such as rainfall, have been observed to enhance gas transfer velocities in laboratory experiments (Liss and Johnson, 2014). However, applying the results from these laboratory experiments into a modified gas transfer velocity within the ETPO region is challenging, and requires further field experiments to validate. It is for this reason, and the role rainfall has in reducing DIC, (thus bringing ΔfCO2 closer to atmospheric equilibrium and limiting the influence on air sea fluxes brought about by an enhanced gas transfer velocity), we do not attempt to correct for the influence rainfall has on air-sea exchanges.

2.3 Satellite observations of SST and SSS

Sea surface temperatures have been continuously measured from space via satellites since the AVHRR mission in 1981, and sea surface salinity has been measured since the launch of the European Space Agency's Soil Moisture and Ocean Salinity (SMOS) satellite mission in November 2009 (Kerr et al. 2010). In this paper, we use satellite T and S data to help in the interpretation of spatial variability of fCO_2 from the ETPO.

SMOS SSS maps at 0.25˚ resolution (running average over $100x100km^2$) produced by the LOCEAN SMOS group (combining SMOS ascending and descending passes) were used within this paper (Boutin et al. 2013, data available at www.cats.ifremer.fr/Products/Availible-products-fromCEC_OS/Locean-v2013). SMOS SSS data are not used prior to June 2010 due to variations in sensor configuration tested during the in-orbit sensor commissioning phase (Corbella et al., 2011). Analysing the accuracy of the SMOS product, using in-situ point observations of SSS can be completed using both SOCAT SSS data (where the salinity is derived from ship mounted thermosalinograph-TSG), and Argo profiles made within the region (S Fig. 1). Binning all Argo and TSG near surface salinity data (that overlaps the SMOS observational period) into the same monthly, 0.25 degree structure as the SMOS monthly 0.25 ˚ product enables direct comparison. It is found that the RMSE between SMOS and these binned in-situ data is 0.24 psu, with a minimal offset (of 0.04 psu, S Fig. 1). This variability is a function of both the intrinsic variability of SSS within the EPTO (for example, caused by localised rainfall, riverine outflow, upwelling events that may occur within each SMOS observational pixel), and a measurement error made in the SMOS data. Estimates of this intrinsic variability within the tropics is 0.1 psu, but in certain regions (such as the western warmpool and ETPO) may feature variabilities of 0.4 psu or higher (Delcroix et al. 2005). If the average intrinsic variability for the Tropical Pacific (of 0.1 psu) is used, the measurement noise within the SMOS product is 0.14 psu. This measurement noise is included in our fCO2 error estimates (as detailed below). We suggest that this is a satisfactory noise to signal ratio, given that the region features SSS variability of upto 8 psu (Fig. 2).

SSS was combined with sea surface temperatures from the operational sea surface temperature and sea ice analysis (OSTIA) system; an optimal interpolation of multiple microwave and infrared satellite-based data sources (Donlon et al., 2012). This SST daily product features a native resolution of 0.05˚, which was subsequently re-sampled over the same spatial and temporal grid as the SMOS data. As auxiliary datasets for near surface T and S, data from the Argo float array were used.

2.4 The basis of using a SST/SSS statistical fCO_2 model in the ETPO

Using an fCO_2 model based on surface T and S properties requires the carbon properties of water masses to be quantified. We define three surface water-masses within the study region, based on the near-surface (0-100 m depth) T and S characteristics of the ETPO recorded by ~6000 Argo profiles between 17 ˚N and 4 ˚N, and east of 95 ˚W (Fig. 2). These water-masses are also independently featured within studies by Kessler (2002, 2006):

1)An ETPO surface water, with temperatures >27˚C and salinities >33.5 (Fig 2. 'B').

2)Deep water that predominantly exists below the thermocline (defined by Kessler as the 20 ˚C isotherm) and is only expressed at the surface of the ETPO during periods of upwelling (Fig 2. 'C').

3)Rain influenced water, with salinities <33.5 (Fig 2. 'A').

Here, the water-mass at ‘C’ (referred to as 'deep water' herein) is predominantly found at depths greater than 80 m, whilst the near surface water is typically ETPO surface water and warmer than 27.5 ˚C (‘A’ and ‘B’). Occasionally, the deep water-mass can be observed at shallower depths, advected upwards during times of strong upwelling (Fig. 2). Rainfall influenced waters display a wide range of salinities (from 29 to 34.5) within the upper 20 m (as observed in the salinity variation between ‘A’ and ‘B’). At low salinities, densities as low as 1018 kg m^{-3} are observed; an eight kg m^{-3} difference between this surface water and deep water (featuring densities of 1026 kg m^3). This large density gradient is an important feature of the ETPO, as periods when stratification and high thermoclines strengths are prevalent, the upwelling of deep water is inhibited (Fiedler and Talley, 2006).

To identify the carbon properties of these water-masses, DIC concentrations between the surface and 100 m depth within the ETPO measured during WOCE transect P19 are shown as red circles and associated concentrations plotted within TS space (Fig. 2). Deep water ‘C’ was observed to have DIC concentrations > 2200 μmol kg^{-1}, contrasting values between ‘A’ and ‘B’ of <1950 μmol kg^{-1}. End-member mixing occurs at intermediate temperatures between the two watermasses ‘B’ and ‘C’, exhibiting in the gradient observed along the 34.2- 34.75 isohalines in figure 2. Assuming that upwelling results in the expression of deep water at the surface, upwelling will act to increase the surface inventory of DIC, leading to increased fCO_2.

Rainfall results in surface layer dilution, thus reducing DIC between ‘A’ and ‘B’ (Turk et al., 2010). When the fCO_2 of both endmembers in this system (rainwater and surface waters) are at equilibrium with the atmosphere, this dilution results in a lowering of fCO_2 within the sea surface, and ingassing of CO_2. Turk et al's (2010) study in the western Pacific warm pool have indicated that decreases of 30- 40 μatm in surface fCO_2 values can result from rainfall alone, with these effects strongest under highly stratified conditions. This suggests that rainfall could be an important influence on ETPO fCO_2, particularly within the rainfall dominated Panama Basin region. Finally, although biological processes influence DIC (and hence fCO_2), observations of DIC within this region suggest that physical processes (such as upwelling or rainfall) are the first order control on DIC. For this reason, coupled to the lack of net community production data within the region, we have elected to concentrate our efforts on quantifying these physical processes.

2.5 Processing SOCAT data

Surface fCO_2 responds to changing levels of atmospheric fCO_2, which is increasing at approximately 20 μatm per decade, (Takahashi et al. 2009, Fig. 3). In order to calculate contemporary air sea fluxes, the multi-year SOCAT data must first be temporally corrected for the inter-annual trend of increasing atmospheric CO_2. The mean annual increase in fCO_2 within the central equatorial Pacific (5 ˚N and 5 ˚S) between 1979 and 1990 (excluding El Niño events) was estimated at a rate of 1.1 µatm +/- 0.3 per year (Takahashi et al., 2009). A second estimate, using data collected between 1990 and 2003 (within the region 10 ˚N to 5 ˚S) calculated an annual increase of 2.0 µatm +/- 0.2 (Takahashi et al. 2009). Correcting 1991 data to contemporary July 2014 values would equate to a not-inconsiderable difference depending on which of these two estimates was chosen. Therefore, in order to choose the optimum correction for the smaller subregion of the ETPO, all available SOCAT fCO_2 data 1991-2011 were binned by year the data was collected (Fig. 3). Fitting a linear regression to the average bin value of this data, resulted in an average annual increase of 1.95 µatm/ yr (+/- 0.38 µatm). This linear regression was found to fall within the 5th and 95th percentile values for all bins, with variability in mean and median values caused by heterogeneous sampling of the region and inter-annual variability (Fig. 3, percentiles plotted in blue). Our calculated rate of increase is both within the range of the annual atmospheric fCO_2 increase measured at Fanning Island (1.8 µatm/ yr +/- 0.1 µatm) suggesting that fCO_2 within the ETPO tracks the rate of increasing atmospheric fCO_2 (Fig. 3). Therefore, we apply a 1.95 µatm per year correction to the SOCAT data in order to normalise the fCO_2 data to 1st July 2014 values, with all results herein also normalised to this date.

Although the spatial distribution of fCO_2 SOCAT observations within the ETPO are irregular, the variability can be constrained once the TS properties of the surface ocean are accounted for (as-per DIC, Fig. 2, Fig. 4). Data from the upper 100 m of Argo profiles completed in each of the three gulfs (Panama, Papagayo and Tehuantepec, as defined in Fig. 1) show strong TS similarities between each of the three gulf regions; low salinity (<34) waters are observed in each gulf, with a thermocline separating surface-water and deep water at 80-100 m depth. The T-S properties of these Argo profiles are replicated at the surface, within SOCAT SST and SSS data (Fig. 4). However, the relative numbers of observations that fall into each water-mass definition is different. The warm ETPO surface water is dominant in all three regions for the majority of samples, but cooler (<20 ºC) deep water is occasionally expressed at the surface, with this signal strongest in the Gulf of Tehuantepec, followed by the Gulf of Papagayo, and seldom observed in the Gulf of Panama. This contrasts observations of low salinity water, which are very frequent within the Gulf of Panama, but rare in the other two gulfs (Fig. 4). Although both SOCAT and Argo data suffer from sparse sampling, we suggest that both datasets indicate that the relative dominance of each water-mass within each of the three gulfs is different. There are very few SOCAT observations within the Offshore (OS) region (Fig. 1), thus we do not show a TS diagram from this region, however Argo profiles from this region are included in Fig. 2, highlighting that the OS also shares the same watermasses as the three gulf regions.

The distribution of DIC concentrations within TS space is mirrored by fCO_2 values; deep water features higher fCO_2 values than ETPO surface water, and low salinity water feature the lowest fCO_2 values. The intermediate values of fCO_2 observed between each of these watermasses suggest end-member mixing of fCO_2 between waters-masses. Finally, there are no watermasses that share TS characteristics, but feature very different DIC concentrations or fCO_2 values, meaning that DIC/ fCO_2 values are unique within TS space in this region (Fig. 2 and 4). Therefore, as both DIC and fCO_2 values behave pseudo-conservatively within TS space, it is possible to construct a statistical description of fCO_2 using solely SSS and SST.

2.6 Fitting a statistical description- the look-up-table

The similarities of T,S and fCO_2 properties of the water-masses observed both by Argo and within the SOCAT database across all three gulfs enable data from the entire ETPO to be considered as a single system (Fig. 5A). As the variance between individual fCO_2 observations occupying the same location within T S space is low (Fig 5B) we use a look-up-table (LUT) to describe fCO_2 as a function of T and S. This LUT technique, although not previously used to estimate oceanic fCO_2 has proven useful for estimating net primary productivity using satellite observations (Zhao et al. 2006). The LUT in this study uses a mesh of equal sized bins within T-S space. Observations of fCO_2 within these discrete TS bins are collected, and an average fCO_2 within TS space calculated. As each bin is fully independent of neighbouring bins, non-linear and/or skewed fCO_2 distributions within TS space can be accounted for, and hence an improved synthetic fCO2 product, with a lower root-mean-squared-error (RMSE) attained compared to using an alternative linear statistical description, such as a basic linear fit.

By combining all SOCAT data from the ETPO onto a single T-S diagram, a look-up-table (LUT) can be produced in order to describe fCO_2 as a function of T and S (Fig. 5). The LUT was constructed by completing a linear interpolation of binned 0.1 (salinity) x 0.1 ˚C SOCAT data from the entire ETPO region. The number of observations per bin is depicted in the right-hand panel. Here, the highest number of observations fall in a narrow region of TS space, between salinities of 32-34.5 and 25-30 ºC (Fig. 5). We tested the quality of fit of the SOCAT based LUT, using LDEO v2013 data. Here fCO_2 values were computed using the LUT using T and S from the LDEO v2013 database, with this computed fCO_2 data compared to the measured (annual increase corrected)

fCO_2 values. The LUT could be applied to 96.2 % of all LDEO v2013 T-S measurements made between 1990 and 2013, with the remaining TS measurements falling outside the TS boundaries of the LUT.

The average root-mean squared error (RMSE) of the LUT was 16.8 µatm between the LUT computed and measured fCO_2. This RMSE was asymmetrically distributed; highest at temperatures of 22-26 ºC/ salinities of 34.4, and lowest at warmer temperatures/ lower salinities and also at colder temperatures (Fig. 5). This suggests that fCO_2 variability is low in aged surface waters, and high in recently upwelled and warming water. As there are a number of measurements within the region of higher error (Fig. 5), we hypothesize that this larger uncertainty is not due to lack of observations, but rather to mixing / heating processes that allow water with slightly different fCO_2 values to occupy the same TS space. For example, the fCO_2 value of water at salinities of 34.5 and 25 ºC could either result from the stoichiometric mixing of two waters at salinities of 34.5, and temperatures of 18 and 32 ºC, or solely from warmed 34.5 /18 ºC water. Upwelling, solar radiation, horizontal advection, biological productivity and diapycnal mixing processes all influence this system, and need to be accounted for in order to quantify completely the formation and fCO_2 observed within this water, but are outside the scope of this study using the data available in this region. However, this LUT technique works efficiently in determining the first-order variability of the system within the ETPO. In order to calculate an uncertainty on this LUT derived synthetic fCO2 data, we complete mean squared error calculation, based on the variance of fCO2 data within each cell of the LUT, and the uncertainty on SMOS SSS (as described above.) We assume that the SST and SSS measurements within SOCAT, and the OSTIA SST product are accurate. This error is propagated through the air-sea flux estimates in order to calculate an error on the air sea flux values (as reported in table 1).

3 Results

3.1 Bi-monthly variability along ship tracks

Bimonthly fCO_2 variability can be seen in the (1991-2011 annual fCO_2 increase corrected) SOCAT observations plotted in figure 6. Here, the top six panels display SOCAT observations of fCO_2, and the lower six panels display fCO_2 calculated from SOCAT SST and SSS observations using the LUT. As the majority of SOCAT data is collected using ships of opportunity, resolution within shipping lanes in the ETPO is excellent; (for example multiple observations are made in regions south and west of the Panama Canal, at 9.1 ºN, 79.7 ºW), but very sparse outside of these shipping lanes. However, acknowledging these issues in data resolution, patterns in fCO_2 can still be detected. The lowest fCO_2 is typically observed within the Gulf of Panama and close to the coast. Higher fCO_2 is observed in the Gulfs of Tehuantepec and Papagayo. Inter seasonal variability is also observed, with the highest fCO_2 (>440 μatm) occurring between November to February, with lower fCO_2 values (<400 μatm) occurring across the entire region during the summer months (May-August). The data also show a very high degree of variability at small spatial and temporal scales, for example during November- December within the Gulf of Papagayo. It is this variability that needs to be resolved using the LUT, when coupled to satellite SST and SSS observations at native resolution. Thus, it is important to confirm that the LUT is able to recreate this variability in fCO_2 using the initial (SOCAT) T and S conditions. Here, we find that the LUT performs well, with most of the measured fCO_2 variability also observed within the fCO_2 calculated using the LUT (Fig. 6).

3.2 fCO_2 and fluxes by region- the influence of wind and upwelling

Using the LUT, SMOS and OSTIA data, the small scale variability and features within the ETPO can be resolved more thoroughly than possible through SOCAT data alone. Bimonthly averaged (between July 2010- June 2014) SSS, SST, fCO_2, CO_2 flux and windspeed are plotted in figure 7. Jet wind velocities over the Gulf of Tehuantepec are at their peak between October to February, thus optimising Ekman upwelling. During these months the SSS of the Gulf increases, whilst the SST decreases (due to the influences of upwelling). Increased fCO_2 is observed across most of the Gulf of Tehuantepec, with peak outgassing occurring as a narrow band, centred underneath the axis of the jet wind. We suggest that this is due to the complimentary nature of ocean physics in this region- high windspeeds promote Ekman upwelling of high DIC deep water, whilst increasing the k component within the air-sea flux parameterisation, thereby maximising CO_2 outgassing.

4 Discussion

The Gulf of Papagayo shares many similarities with the Tehuantepec Gulf, however, jet winds are more zonally aligned (reducing Ekman pumping strengths, (Alexander et al., 2012)), and occur later into winter compared to Tehuantepec; being strongest between November-February. This results in a lag between peak wintertime fCO_2 values seen within the two gulfs (Fig. 7 and 8). The Gulf of Papagayo also features elevated fCO_2 values during the summer months which are not seen in either the Gulf of Tehuantepec or Panama. This is due to westerly winds maintaining the vorticity of the Costa Rican dome structure, enabling the continued upwelling of deep water at the core of this dome throughout the summer season (Grodsky et al. 2014, Kessler 2006, Fig. 7).

The seasonally averaged wind velocities in the Gulf of Panama superficially resemble the wind patterns in the two northern gulfs- jet winds are observed between January- February (Fig. 7). However, excluding a small area of ocean directly underneath the wind jet axis during winter, the region remains a small net sink of carbon throughout the year (Fig. 8). We suggest that this contrast between the Panama gulf and the rest of the ETPO is due to the high rainfall within this region, resulting in the dilution of DIC as described above.

4.1 fCO_2 and the influence of rainfall

A significant proportion of atmospheric water exported from above the Atlantic basin into the Pacific basin is precipitated into the ETPO. This rainfall is intensified within the ETPO during the summertime, due to a northwards shift of the ITCZ towards the Panama coast (Xie et al., 2005). As a result, the Gulf of Panama receives net precipitation of 180-220 cm per year, with peak rainfall of 20 mm per day during July- August (Alory et al., 2012). This large freshwater flux, coupled with light southerly winds between March and June, and the southerly (thus downwelling promoting), winds between July and December result in the semi-permanent stratification of the water-column (Fig. 7, Alory et al., 2012). Qualitatively, this stratification can be observed in the SOCAT and Argo data in Fig. 4 by the scarcity of deep water observations in the Gulf of Panama compared to the Gulfs of Tehuantepec and Papagayo. Additionally, the thermocline is observed at deeper depths in the Argo profiles taken in the Gulf of Panama, compared to either the Gulf of Tehuantepec or Papagayo (Fig. 4).

The influence of stratification/ rainfall on fCO_2 values are seen in figure 7. Here, the lowest salinity and fCO_2 are observed during the summer months (during peak rainfall season, Alory et al. 2012). This low fCO_2, stratified system persists until January, when intensification of the south equatorial current results in the export of the low fCO_2/fresh surface layer towards the south west (as seen by the elongation of the freshpool during January- March SSS). This export of water, coupled with the dry-season within the Panama Gulf appears to weaken the stratification, with the result that sporadic jet winds enable Ekman upwelling, thus increasing SSS (Alory et al., 2012, Fig. 7) and average fCO_2 values between January-April (Fig. 8).

4.2 Air-sea fluxes from July 2010- June 2014

The ETPO between 2010- June 2014 had an annual average ΔfCO_2 39.4 µatm (+/- 10.7) and a outgassing CO_2 flux of 1.51 mmol $m^{-2}\ d^{-1}$ (+/-0.41 , Fig. 8/ Table 1). The ETPO, (the boundaries of which defined as per Fig. 1), has an area of 1.9 $x10^{12}m^2$, therefore, net outgassing from the ETPO equates to 10 $x10^{12}$ g (0.01 Pg) of carbon per year.

To examine both monthly and inter-annual variability in air-sea fluxes, the ETPO is split into subregions; the Gulfs of Tehuantepec, Papagayo, Panama and the Offshore region (Fig. 1, 8 and Table 1). Here, although variable, the consistent seasonal cycle between summer and winter observed in the bimonthly data in figure 7 is present for each individual year. Peak outgassing within the Gulfs of Tehuantepec, Papagayo and the South Equatorial Current occurs during winter (November -February). This contrasts the Gulf of Panama, which is a net sink of atmospheric CO_2 except during occasional upwelling events during January -February. However, ingassing within of the Gulf of Panama is insufficient to offset outgassing from the rest of the ETPO and the region remains a net source of CO_2 year round.

In addition to seasonal variability, interannual variability is observed within the ETPO. Across the entire basin, the ETPO during the years 2010-2012 were on average cooler and saltier than subsequent years (especially 2012-13). This resulted in higher annually averaged outgassing and fCO_2 values (Fig. 8, Table 1). Concurrently, during 2010-2012, the Gulf of Panama featured a low salinity mimima (of 28), and a small freshpool footprint (the boundary of which is defined by the 33 isohaline (Alory et al., 2012)). The extreme low salinity observed within the eastern region of Gulf of Panama during 2010 to 2012 resulted in lower fCO_2 and hence stronger ingassing than 2012-2014 values, highlighting the effect of rainwater dilution of DIC. However, this localised ingassing was insufficient to offset the higher outgassing observed in the other regions of the ETPO (Fig. 8, Table 1). Also noteworthy is that average wind velocities were similar during 2010 and 2012 compared to subsequent years, so the increased outgassing observed during these years cannot be attributed to increased wind-mediated Ekman upwelling of deep water alone.

We note that 2010 to the end of 2011 featured La Niña conditions, and suggest that this could be causal to the differences in CO_2 fluxes, higher salinities and higher fCO_2 observed during this time period. A study using NCEP (National Centers for Environmental Prediction) reanalysis data within this region observed cooler waters and more frequent upwelling of sub-thermocline deep water during La Niña events. A shallower thermocline depth exists during La Niña events, which results from the uplift of the water-column by intensified coastal Kelvin waves. Mechanistically, this shallow thermocline reduces the strength of upwelling required for the expression of deep water at the surface, thus decreasing average SSTs observed during La Niña periods (Alexander et al., 2012).

Furthermore, Alexander et al's (2012) study also suggests that although jet winds are the first order control on SST and thermocline depth during winter; it is changes in the thermocline depth (rather than changes in jet winds) that result in observed El Nino Southern Oscillation (ENSO) variability in SST within the ETPO. Variability in thermocline depth, and by association, variability in the ease by which deep water can be advected towards the surface suggest that (ENSO) could drive variability within the surface fCO_2 observations. However, with only four years of data, and no El Niño phase for intercomparision we are unable to draw definitive conclusions.

4.3 Previous work

The results in figures 7 and 8 represent the first attempt to quantify fCO_2 within the ETPO region at high resolution from observations. Previous work encompassing the ETPO include three basin wide or global fCO_2/ pCO_2 studies, by Takahashi et al., (2009), Ischii et al., (2014) and Landschützer et al., (2014). These studies, as discussed in the introduction, are based on the extrapolation of pCO_2 directly, or the extrapolation of pCO_2 using a neural network technique, and feature spatial resolutions of 4° x 5°, 4 °x 5° and 1° x 1° respectively. Of these three studies, only Takahashi et al. (2009) features a dataset of calculated ΔpCO_2 that includes the ETPO region, thus allowing direct comparison with our calculations. Collocating the ΔpCO_2 results from Takahashi et al. (2009) within the ETPO regions defined in Fig. 1, the Gulfs of Techuantepec, Papagayo, Panama and the Offshore region featured values of +28.9, +54.1, +17.1 and +19.5 µatm respectively (Table. 1). This suggests that the Takahashi et al. (2009) study differentiates the low ΔpCO_2 Panama Gulf region from the higher values observed in the Gulfs of Tehuantepec and Papagayo. The resolution used in Takahashi's study is too coarse to identify any mesoscale features (such as upwelling), or interannual variability within the region. However, we find average ΔpCO_2 from Takahashi et al. (2009) of 29.1 µatm was within the error limits of this study (Table 1).
Applying the same windspeed product, and gas transfer parametrisation used in this study to the ETPO ΔpCO_2 values from Takahashi et al. (2009), we find that all regions are net outgassing, with the Gulf of Papagayo dominant within the ETPO (table 1). The ingassing observed within the Gulf of Panama for our study is not replicated in Takahashi et al. 2009. The improved resolutions featured in Landschützer et al., (2014) resulted in some mesoscale features being observed, such as the increased pCO_2 values within the Gulf of Papagayo. However, this work was not able to identify the low pCO_2 conditions within the Gulf of Panama, most likely due to the same biogeochemical province description being applied to the entire ETPO. In addition to these studies, our work distinguishes the importance of jet winds in increasing pCO_2, and quantifies the strong inter annual variability within the region.

5. Conclusions

Estimating surface fCO_2 and air sea fluxes of CO_2 within the global oceans has advanced considerably over the past decade, assisted by the assembly of large standardised atlases of surface observations (such as the SOCAT database). However, although these databases boast measurements in the millions, a challenge remains in gauging seasonal or sub-mesoscale fCO_2 variability in the oceans. Sampling through the use of commercial volunteering observation vessels may introduce bias, with most data existing within the narrow confines of the major global shipping lanes or for only a few months of the year. However, the quantification of fCO_2 within TS space, used in conjunction with observations of surface SST and SSS (made possible through the recent availability of SSS from satellite) has proved highly useful in improving our understanding of fCO_2 variability at much improved spatial and temporal resolutions. We have demonstrated a technique using SOCAT data to identify the fCO_2 signatures of water-masses within the ETPO region, namely, the high fCO_2 deep water, the near equilibrium ETPO surface water, and the undersaturated rainfall diluted surface waters. From this, we used a LUT technique, in order to produce a description of the fCO_2 content of an ETPO surface water using satellite SST and SSS. The highest outgassing and surface fCO_2 were observed during the winter period (November -March), in the Gulfs of Tehuantepec, Papagayo and in the south equatorial current. The first order control on these upwelling events and hence fCO_2 in the ETPO are strong wind jets blowing through low altitude gaps in the Central American cordillera. The Gulf of Panama remained net undersaturated on average, due to dilution effects of heavy rainfall and the stratification of the water column. Although wind jets were observed in the Gulf of Panama, the exceptionally low density of the water within this region appears to limit upwelling, and any upwelling that occurs is directly underneath the wind jet axis. Inter-annual variability was observed within the region, with the location of the western extent of the freshpool moving westwards considerably between 2010 and 2014. Previous work within this region suggest that changes in thermocline depth related to ENSO are likely to influence fCO_2 within this region. The region is a net contributor to atmospheric CO_2, with average sea to air fluxes (over the four years of observations) of 1.5 mmol m^{-2} d^{-1}, with all regions of the ETPO outgassing year-round, except the rainfall diluted Gulf of Panama/ Freshpool region.

Acknowledgements

The research leading to these results was aided by the LOCEAN team Xiaobin Yin and Nicolas Martin, and supported through the EU FP7project CARBOCHANGE Changes in carbon uptake and emissions by oceans in a changing climate which received funding from the European Commission's Seventh Framework Programme under grant agreement no. 264879 and the SMOS+SOS STSE project funded by ESA .

We would also like to thank all of the contributors to SOCAT and LDEO of fCO_2/ pCO_2 observations within the Pacific Ocean, specifically Yukihiro Nojiri, Taro Takahashi and Richard Feely who contributed greatly within this region. Finally, we would like to thank the anonymous reviewer and Rik Wanninkhof for their insightful reviews.

References

Alexander, M. a., H. Seo, S. P. Xie, and J. D. Scott (2012), ENSO's Impact on the Gap Wind Regions of the Eastern Tropical Pacific Ocean, J. Clim., 25(10), 3549–3565,

Alory, G., C. Maes, T. Delcroix, N. Reul, and S. Illig (2012), Seasonal dynamics of sea surface salinity off Panama: The far Eastern Pacific Fresh Pool, J. Geophys. Res., 117(C4), C04028,

Bakker, D. C. E. et al. (2014), An update to the Surface Ocean CO2 Atlas (SOCAT version 2), Earth Syst. Sci. Data, 6(1), 69–90,

Boutin, J., J. Etcheto, and Y. Dandonneau (1999), Satellite sea surface temperature: a powerful tool for interpreting in situ pCO2 measurements in the equatorial Pacific Ocean, Tellus B, 51B, 490–508.

Boutin, J., N. Martin, G. Reverdin, X. Yin, and F. Gaillard (2013), Sea surface freshening inferred from SMOS and ARGO salinity: impact of rain, Ocean Science, 9(1), 183-192, doi:10.5194/os-9-183-2013.

Chelton, D. B., Esbensen, S. K., Schlax, M. G., Thum, N., Freilich, M. H., Wentz, F. J., ... & Schopf, P. S. (2001). Observations of coupling between surface wind stress and sea surface temperature in the eastern tropical Pacific,.Journal of Climate, 14(7), 1479-1498.

Corbella, I., F. Torres, N. Duffo, V. González-Gambau, M. Pablos, I. Duran, and M. Martín-Neira
(2011), MIRAS Calibration and Performance: Results From the SMOS In-Orbit Commissioning Phase, IEEE Trans. Geosci. Remote Sens., 49(9), 3147–3155,

Cosca, C. E., R. A. Feely, J. Boutin, J. Etcheto, M. J. McPhaden, F. P. Chavez, and P. G. Strutton (2003), Seasonal and interannual CO2 fluxes for the central and eastern equatorial Pacific Ocean as determined from fCO2-SST relationships, Journal of Geophysical Research: Oceans, 108(C8), 3278.

Donlon, Craig J., Matthew Martin, John Stark, Jonah Roberts-Jones, Emma Fiedler, and Werenfrid Wimmer. "The operational sea surface temperature and sea ice analysis (OSTIA) system." Remote Sensing of Environment 116 (2012): 140-158.

Feely, R. A., T. Takahashi, R. Wanninkhof, M. J. McPhaden, C. E. Cosca, S. C. Sutherland, and M.-E. Carr (2006), Decadal variability of the air-sea CO2 fluxes in the equatorial Pacific Ocean, J. Geophys. Res., 111.

Fiedler, P. C., and L. D. Talley (2006), Hydrography of the eastern tropical Pacific: A review, Prog. Oceanogr., 69(2-4), 143–180, doi:10.1016/j.pocean.2006.03.008.

Grodsky, S. A., J. A. Carton, and A. Bentamy (2014), Salty anomalies forced by Tehuantepec and Papagayo gap winds: Aquarius observations, Remote Sensing Letters, 5(6), 568-574, doi:10.1080/2150704X.2014.935522.

Ishii, M. et al. (2014), Air–sea CO2 flux in the Pacific Ocean for the period 1990–2009, Biogeosciences, 11(3), 709–734

Kessler, W. (2002), Mean three-dimensional circulation in the northeast tropical Pacific, J. Phys. Oceanogr., 2457–2471.

Kessler, W. S. (2006), The circulation of the eastern tropical Pacific: A review, Prog. Oceanogr., 69(2-4), 181–217

Kerr, Y. H., et al. (2010), The SMOS mission: New tool for monitoring key elements of the global water cycle, Proc. IEEE, 98(5),666–687.

Landschützer, P., N. Gruber, D. C. E. Bakker, and U. Schuster (2014), Recent variability of the global ocean carbon sink, Global Biogeochemical Cycles, , 1–23.

Le Quéré, Corinne, R. Moriarty, R. M. Andrew, G. P. Peters, Philippe Ciais, Pierre Friedlingstein,

S.D. Jones et al. "Global carbon budget 2014." Earth System Science Data Discussions 7, no. 2 (2014): 521-610.

Park, G.-H., R. I. K. Wanninkhof, S. C. Doney, T. Takahashi, K. Lee, R. A. Feely, C. L. Sabine, J. TriÑAnes, and I. D. Lima (2010), Variability of global net sea–air CO2 fluxes over the last three decades using empirical relationships, Tellus B, 62(5), 352-368, doi:10.1111/j.16000889.2010.00498.x.

Rangama, Y., J. Boutin, J. Etcheto, L. Merlivat, T. Takahashi, B. Delille, M. Frankignoulle, and D. C. E. Bakker (2005), Variability of the net air–sea CO2 flux inferred from shipboard and satellite measurements in the Southern Ocean south of Tasmania and New Zealand, Journal of Geophysical Research: Oceans, 110(C9), C09005, doi:10.1029/2004JC002619.

Reul, N., et al. (2013), Sea Surface Salinity Observations from Space with the SMOS Satellite: A New Means to Monitor the Marine Branch of the Water Cycle, Surv Geophys, 35(3), 681-722, doi:10.1007/s10712-013-9244-0.

Rödenbeck, C., R. F. Keeling, D. C. E. Bakker, N. Metzl, a. Olsen, C. Sabine, and M. Heimann (2013), Global surface-ocean p^{CO}2 and sea–air CO2 flux variability from an observationdriven ocean mixed-layer scheme, Ocean Sci., 9(2), 193–216,

Rödenbeck, C., Bakker, D. C. E., Metzl, N., Olsen, A., Sabine, C., Cassar, N., Reum, F., Keeling, R. F., and Heimann, M.: Interannual sea–air CO2 flux variability from an observation-driven ocean mixed-layer scheme, Biogeosciences, 11, 4599-4613, doi:10.5194/bg-11-4599-2014, 2014.

Takahashi, T. et al. (2009), Climatological mean and decadal change in surface ocean pCO2, and net sea–air CO2 flux over the global oceans, Deep Sea Res. Part II Top. Stud. Oceanogr., 56(8-10), 554–577

Takahashi, T., S. C. Sutherland, D. W. Chipman, J. G. Goddard, and C. Ho (2014), Climatological distributions of pH, pCO2, total CO2, alkalinity, and CaCO3 saturation in the global surface ocean, and temporal changes at selected locations, Mar. Chem., 164, 95–125,

Turk, D., C. J. Zappa, C. S. Meinen, J. R. Christian, D. T. Ho, A. G. Dickson, and W. R.

McGillis (2010), Rain impacts on CO 2 exchange in the western equatorial Pacific Ocean, Geophys. Res. Lett., 37(23),

Weiss, R. F. 1974. Carbon dioxide in water and seawater: The solubility of a nonideal gas. Marine Chemistry 2: 203-215.

Xie, S.-P., H. Xu, W. S. Kessler, and M. Nonaka (2005), Air–Sea Interaction over the Eastern Pacific Warm Pool: Gap Winds, Thermocline Dome, and Atmospheric Convection, J. Clim., 18(1), 5–20,

Zhao, M., Heinsch, F. A., Nemani, R. R., & Running, S. W. (2005). Improvements of the MODIS terrestrial gross and net primary production global data set. *Remote sensing of Environment*, *95*(2), 164-176.

Figure

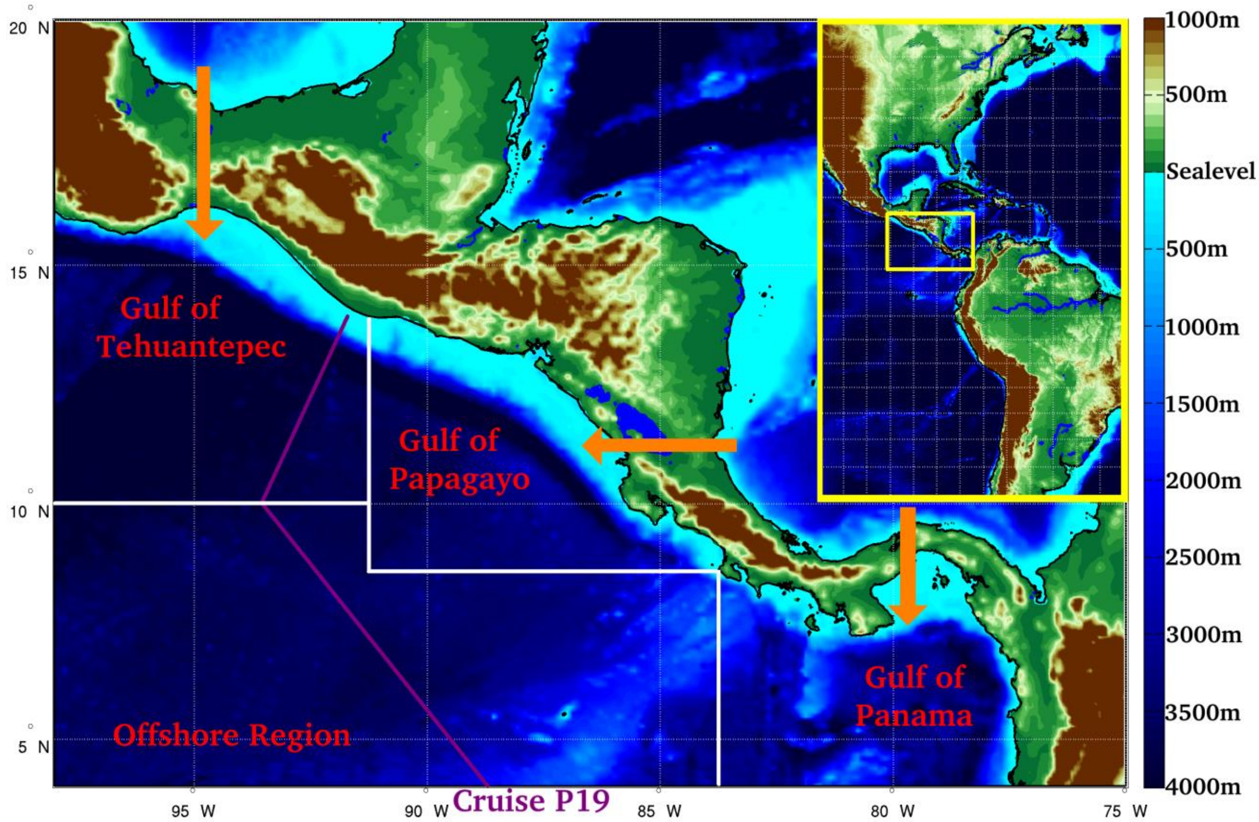

Figure 1.

The topography of the Eastern Tropical Pacific Ocean and Isthmus of Panama, plotted using GEBCO bathymetry. The three gulfs with the region, Panama (84° W to coastline of panama), Papagayo (84 to 91 °W, north of 8 °N) and Tehuantepec (west of 91 °W, north of 10 °N), and the Offshore region are marked in white. The transect of WOCE cruise P19 is indicated in purple. The path of jet winds are marked by orange arrows.

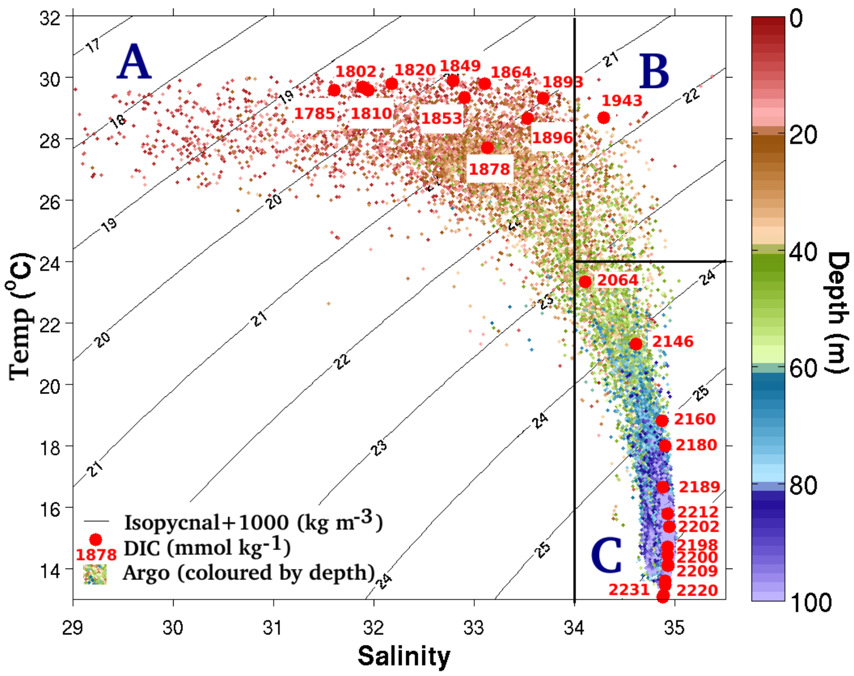

Figure 2.

The total library of Argo profiles collected within the ETPO in the upper 100 metres. Numbered red dots indicate the total dissolved carbon concentration at specific TS values as measured during cruise WOCE cruise p19.

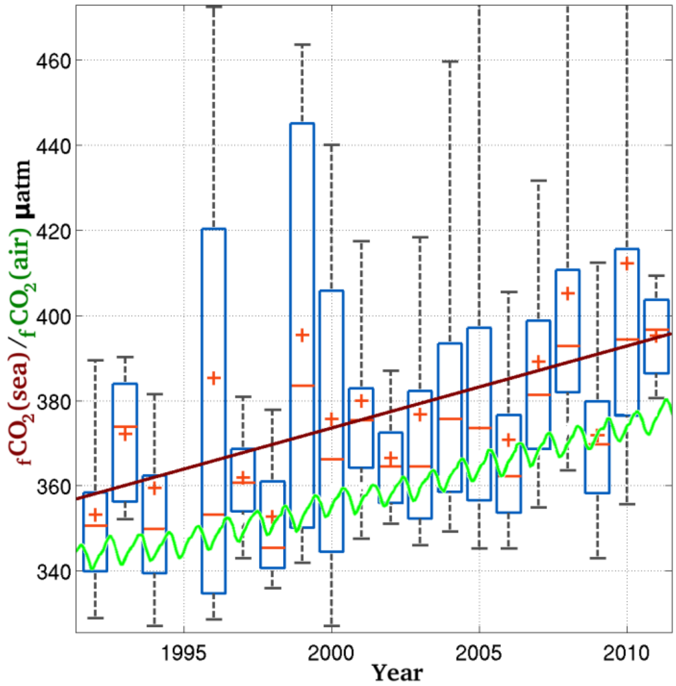

Figure 3.

Yearly binned pCO_2 measurements from the SOCAT database. The interpolated average rate of ETPO fCO_2 increase is shown as a red line, with the atmospheric fCO_2 data shown as a green line. The blue boxes represent the 5th and 95th percentile pCO_2, with the small red lines indicating yearly averages, and the red crosses yearly median.

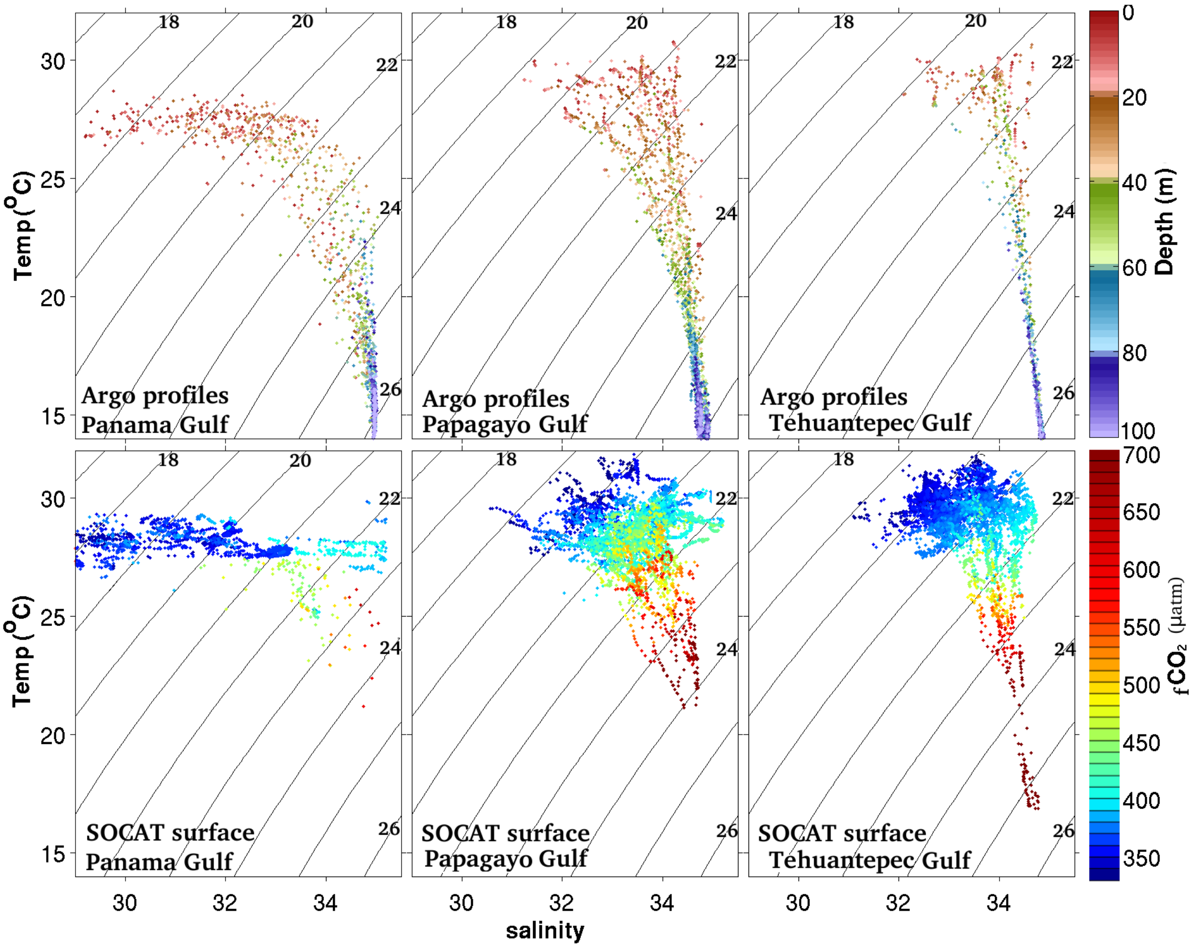

Figure 4.

TS data from the three main gulfs within the ETPO both from Argo floats (coloured by depth-top three plots) and from surface SOCAT T and S data, (coloured by fCO_2 -bottom three plots).

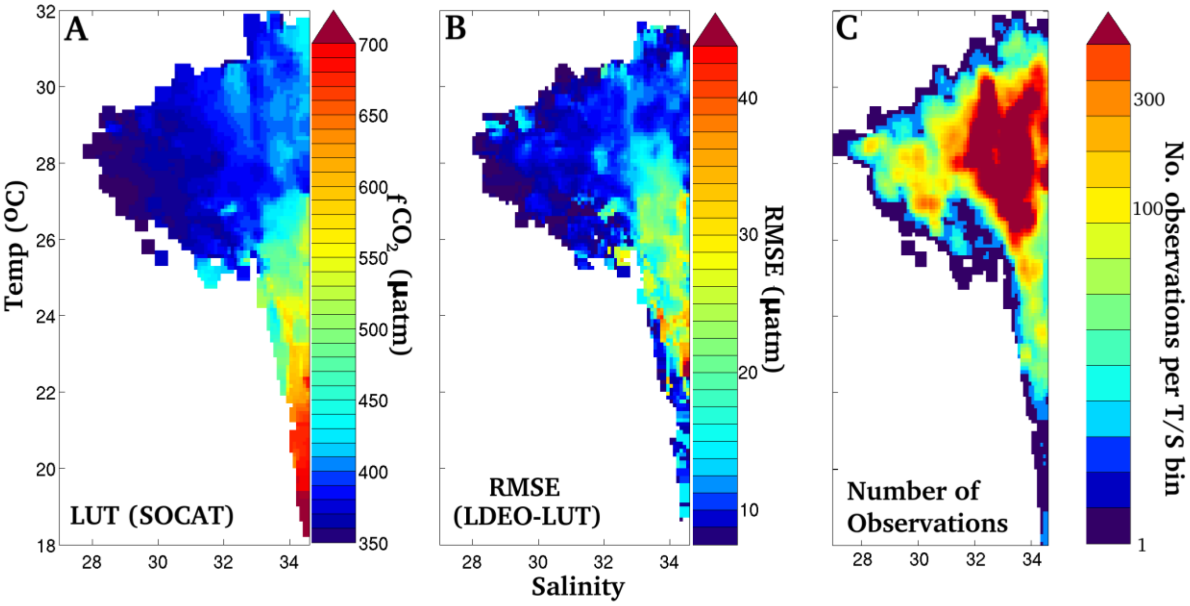

Figure 5.

A, the Look Up Table derived from the position of ETPO SOCAT fCO_2 measurements within T S space.

B the root mean squared error of the LUT –fCO_2 observations, showing the variance between fCO_2 observed within the same TS space in the LUT.

C the number of LDEO measurements per 0.1° x 0.1° salinity/ temperature bins that went into generating the LUT

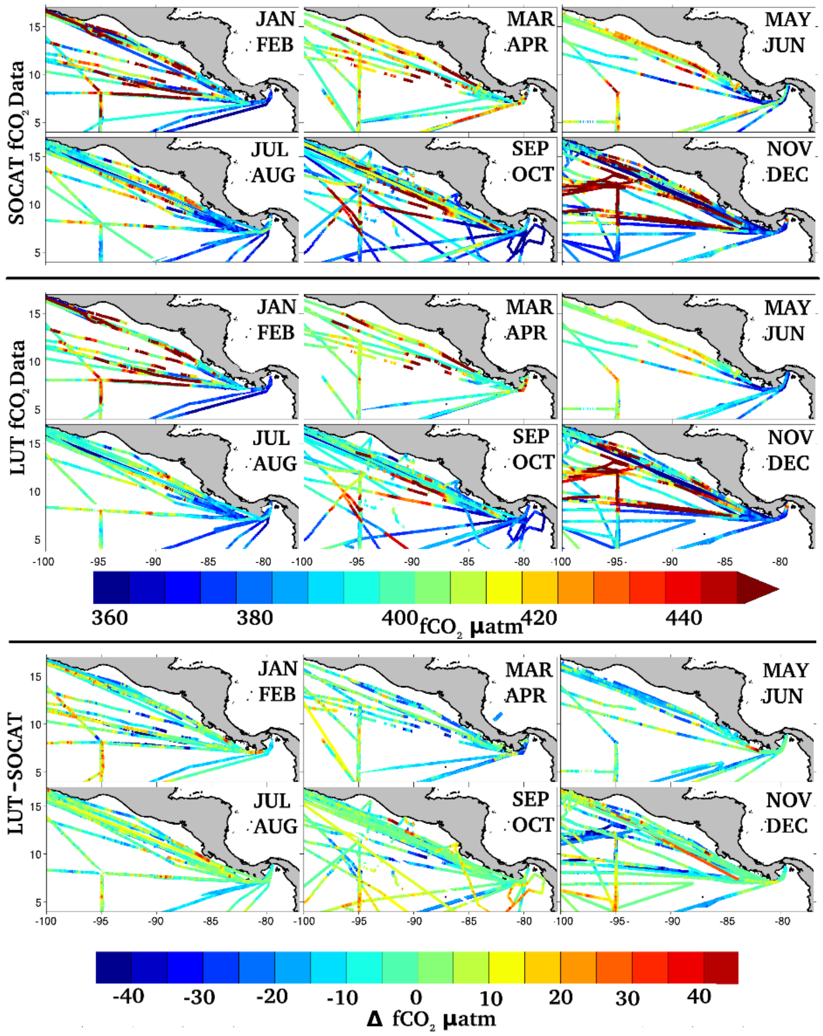

Figure 6.

SOCAT fCO_2 bimonthly (Jan+Feb, Mar+Apr, May+Jun, Jul+Aug, Sep+Oct, Nov+Dec) observations within the ETPO corrected for the annual CO2 increas, LUT derived bimonthly fCO_2 calculated using SOCAT SST and SSS observations and LUT-SOCAT observations

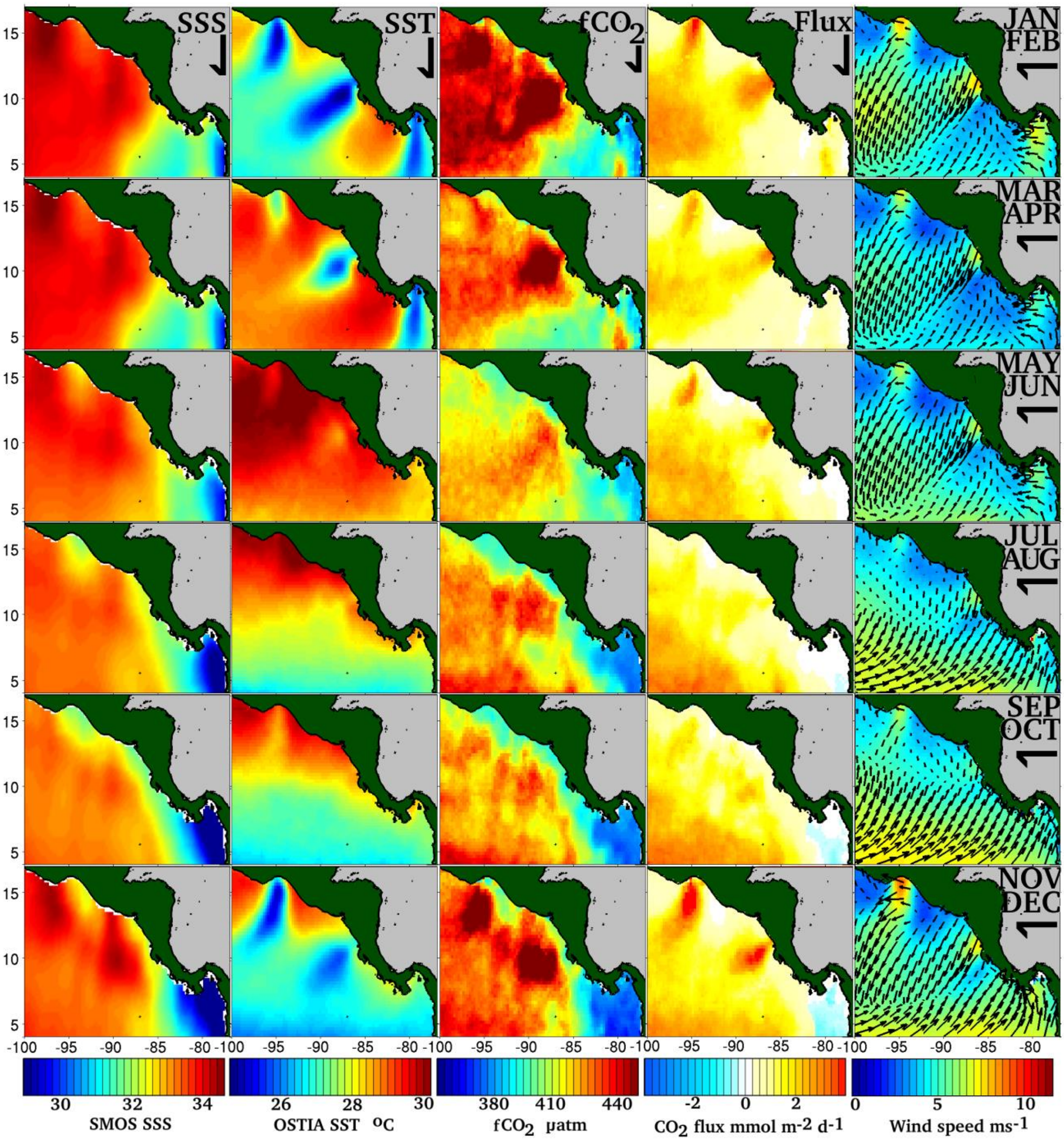

Figure 7.

July 2010- June 2014 average SSS, SST, LUT derived fCO_2 , air sea fluxes and wind vectors for the ETPO, split bimonthly (Jan+Feb, Mar+Apr, May+Jun, Jul+Aug, Sep+Oct, Nov+Dec).

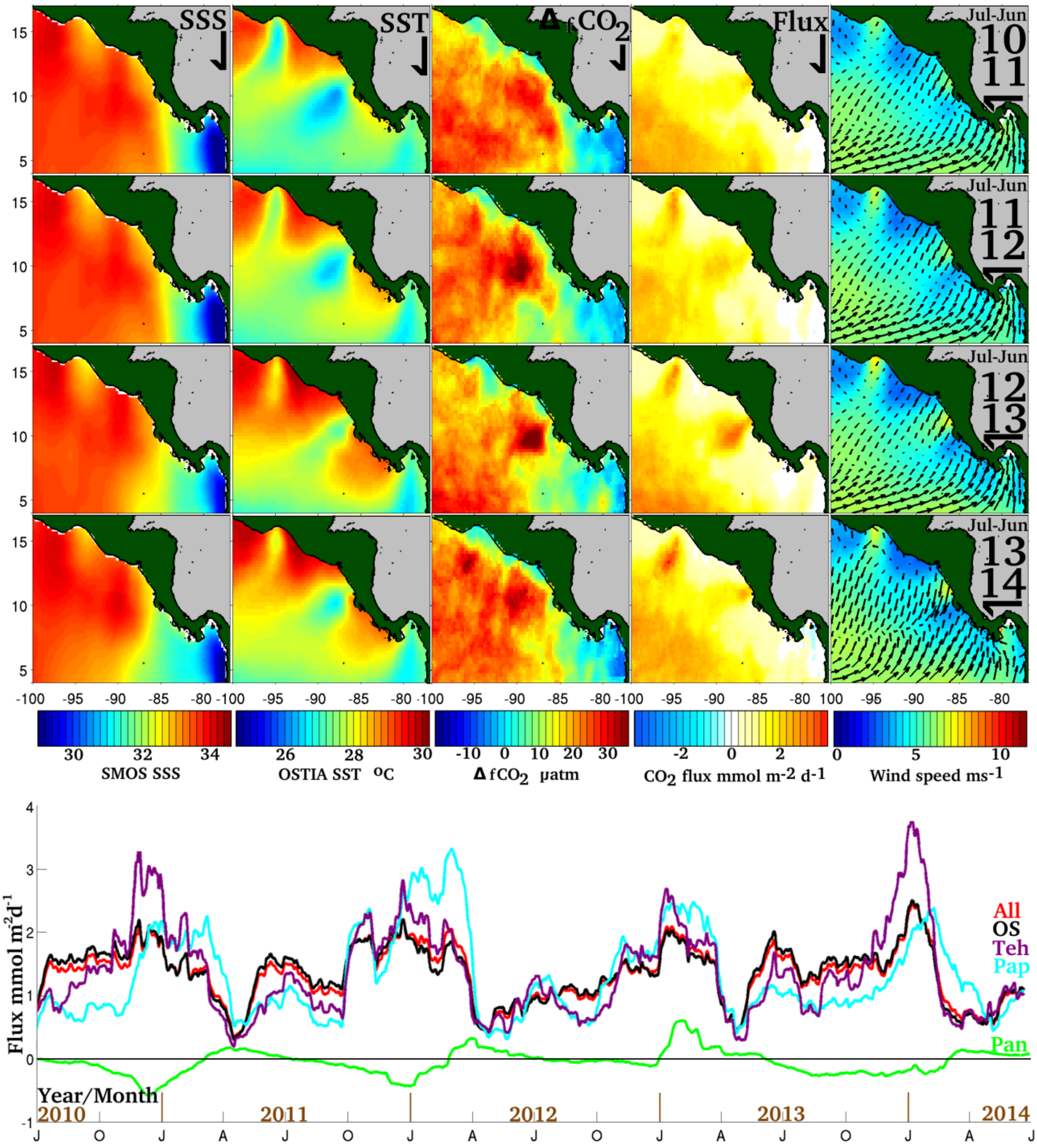

Figure 8.

Upper: Yearly average SSS, SST LUT derived ΔfCO_2 , air sea fluxes and wind vectors for the ETPO for July to June 2010+2011, 2011+2012, 2012+2013 and 2013+2014.

Lower: The continuous LUT derived fCO_2 fluxes from the entire ETPO (red line), the Gulfs of Tehuantepec (purple), Papagayo (blue), Panama (green) and the South Equatorial Current (black).

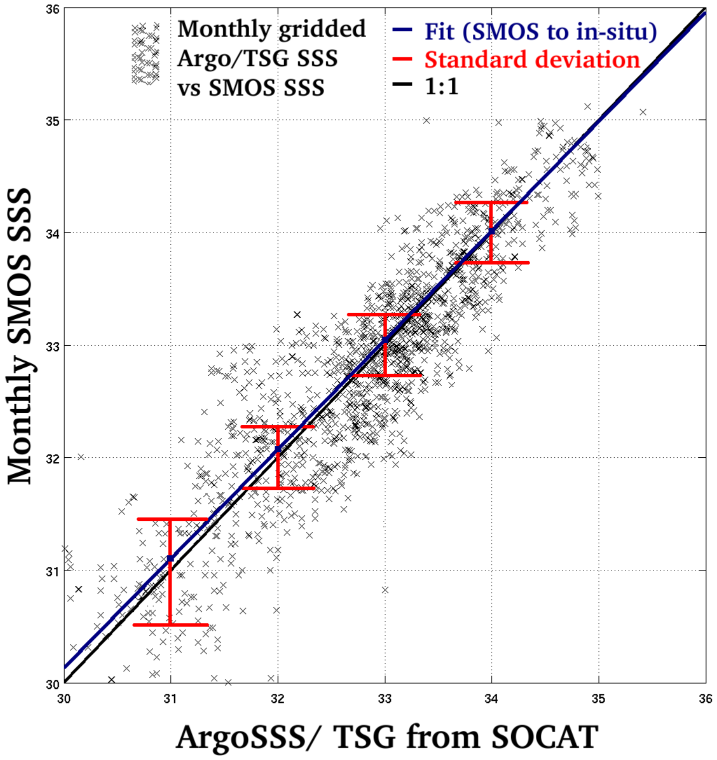

Supplementary Figure 1.

Monthly 0.25 degree SMOS SSS matchups with near surface Argo and SOCAT TSG data (that have been binned into the same monthly/ 0.25 degree grid as the SMOS SSS data). The red error bars indicate the standard deviation, the blue line is a linear regression between the two SSS datasets.

Table 1.
Annual averaged values for each region, as reported in figure 8 and average values from Takahashi et al. 2009.

Date/ Location	Δ fCO_2 (µatm)	CO_2 Flux (mmol m-2 d-1)	CO_2 Flux error (+/- mmol m-2 d-1)	Wind (ms-2)	Salinity	Temp (ºC)
2010-11 ETPO	40.4	1.55	0.39	4.81	33.3	27.9
2010-11 OS	41.1	1.62	0.40	5.18	33.2	27.7
2010-11 Panama	-4.7	-0.19	-0.03	4.57	28.3	27.4
2010-11 Papagayo	34.8	0.95	0.20	4.17	33.7	28.2
2010-11 Tehuantepec	40	1.55	0.33	3.72	33.6	29.0
2011-12 ETPO	42	1.56	0.43	4.59	33.3	27.9
2011-12 OS	43.2	1.60	0.48	4.97	33.1	27.7
2011-12 Panama	-4.1	-0.21	0.05	4.02	28.4	27.5
2011-12 Papagayo	34.1	1.09	0.34	4.01	33.7	27.9
2011-12 Tehuantepec	49.3	1.64	0.36	3.90	33.7	28.4
2012-13 ETPO	35.3	1.41	0.40	4.88	33.2	28.6
2012-13 OS	37.1	1.50	0.43	5.11	33.0	28.3
2012-13 Panama	-2.1	-0.11	0.08	3.92	28.7	27.3
2012-13 Papagayo	32.8	1.08	0.37	4.49	33.6	28.5
2012-13 Tehuantepec	32.5	1.52	0.43	4.08	33.6	29.3
2013-14 ETPO	39.9	1.53	0.41	4.67	33.3	28.0
2013-14 OS	39.3	1.63	0.45	5.09	33.0	27.8
2013-14 Panama	-2.8	-0.16	0.05	3.88	27.5	27.7
2013-14 Papagayo	37.9	1.15	0.38	4.15	33.7	28.0
2013-14 Tehuantepec	47.7	1.57	0.43	3.92	33.7	28.6
Average ETPO	39.4	1.51	0.41	4.7	33.3	28.10
Average OS	40.2	1.59	0.44	5.1	33.1	27.88
Average Panama	-3.4	-0.17	0.04	4.1	28.2	27.48
Average Papagayo	34.9	1.07	0.32	4.2	33.7	28.15
Average Tehuantepec	42.4	1.57	0.42	3.91	33.7	28.83
Takahashi 2009. ETPO	29.1	0.78	N/A	4.74	33.3	28.10
Takahashi 2009. OS	19.5	0.65	N/A	5.09	33.1	27.88
Takahashi 2009. Pan	17.1	0.54	N/A	4.10	28.2	27.48
Takahashi 2009. Pap	54.1	1.83	N/A	4.21	33.7	28.15
Takahashi 2009. Tec	28.9	0.71	N/A	3.91	33.7	28.83